Optical properties and London dispersion interaction of amorphous and crystalline SiO_2 determined by vacuum ultraviolet spectroscopy and spectroscopic ellipsometry

G. L. Tan,[1] M. F. Lemon,[2] D. J. Jones,[2] and R. H. French[1,2,*]
[1]*Department of Materials Science and Engineering, University of Pennsylvania, Philadelphia, Pennsylvania 19104, USA*
[2]*DuPont Central Research, E356-384 Experimental Station, Wilmington, Delaware 19880, USA*
(Received 18 October 2004; revised manuscript received 1 April 2005; published 16 November 2005)

The interband optical properties of crystalline (quartz) and amorphous SiO_2 in the vacuum ultraviolet (VUV) region have been investigated using combined spectroscopic ellipsometry and VUV spectroscopy. Over the range of 1.5–42 eV the optical properties exhibit similar exciton and interband transitions, with crystalline SiO_2 exhibiting larger transition strengths and index of refraction. Crystalline SiO_2 has more sharp features in the interband transition strength spectrum than amorphous SiO_2, the energy of the absorption edge for crystalline SiO_2 is about 1 eV higher than that for amorphous SiO_2, and the direct band-gap energies for *X*-cut and *Z*-cut quartz are 8.30 and 8.29 eV within the absorption coefficient range 2–20 cm^{-1}. In crystalline SiO_2 we report different interband transition peaks at 16.2, 20.1, 21, 22.6, and 27.5 eV, which are in addition to those lower energy transitions previously reported at 10.4, 11.6, 14, and 17.1 eV. We find the bulk plasmon energy in *X*- and *Z*-cut crystalline quartz and amorphous SiO_2 to be at 24.6, 25.2, and 23.7 eV, respectively. The oscillator strength (f) sum rules of the interband transitions for crystalline SiO_2 is 10–10.8 electrons per formula unit for transition energies up to 45 eV. These differences in the electronic structure and optical properties, and the physical densities of crystalline and amorphous SiO_2, can be attributed to differences in the intermediate-range order (IRO) and long-range order (LRO) of the different forms of SiO_2. The intimate relationship between the electronic structure and optical properties and the London dispersion interaction has attracted increased interest recently, and the role of amorphous silica and other structural glass formers as a fluid in high-temperature wetting and materials processes means a detailed knowledge of the optical properties and London dispersion interaction in SiO_2 is important. Hamaker constants for the London dispersion interaction of the configuration of two layers of c-SiO_2 or a-SiO_2 separated by an interlayer film have been determined, using full spectral methods, from the interband transition strength. The London dispersion interaction is appreciably larger in c-SiO_2 than a-SiO_2 due to the increased physical density, index of refraction, transition strengths, and oscillator strengths in quartz.

DOI: 10.1103/PhysRevB.72.205117 PACS number(s): 78.40.−q, 78.20.Ci

I. INTRODUCTION

Because of their similar atomic structure, the study of the optical properties of crystalline SiO_2 (c-SiO_2; α-quartz) and amorphous SiO_2 (a-SiO_2; ultrahigh-purity fused silica) helps elucidate the electronic structure of the different forms. There has been an extensive amount of experimental electronic structure work on SiO_2, including measurements of x-ray emission and absorption spectra,[1] x-ray (XPS) and ultraviolet photoelectron emission (UPS) spectra,[2,3] low-energy electron-loss spectra,[4] photoconductivity,[5] and optical reflectivity.[6,7] From the conductivity measurements,[5] a band gap of ~9 eV has been deduced for a-SiO_2 and by comparison, the XPS data[8] for a-SiO_2 and c-SiO_2 shows ~0.5 eV larger band gap in c-SiO_2. On the other hand, the reflectivity spectra of c-SiO_2 and a-SiO_2 have been shown to be similar,[6] indicating that the electronic structure of a-SiO_2 and c-SiO_2 are quite comparable. To more quantitatively compare similarities and differences arising from the atomic structures of a-SiO_2 and c-SiO_2, we have used Kramers-Kronig analysis[9] of vacuum ultraviolet (VUV) reflectance coupled with spectroscopic ellipsometry.

The physical density of c-SiO_2 at 2.648 (g/cm^3) (Ref. 10) is much higher than that of a-SiO_2 at 2.196 (g/cm^3).[10] The short-range order (SRO) of a-SiO_2 is the same as in the 4:2 coordinated crystals. However, it is the intermediate range order (IRO) and the lack of long-range order (LRO) that distinguished the a-SiO_2 from its c-SiO_2 counterpart. It has been assumed that the electronic structure of a-SiO_2 is similar to that of c-SiO_2.[11] It had been reported that the calculated electronic density of states (DOS) of c-SiO_2 and a-SiO_2 have subtle differences,[12,13] reflecting the long-range-order (LRO) and intermediate-range order (IRO) of these two phases, in spite of the similarity in their short-range order (SRO).[12] But these subtle differences of the DOS between two phases appear to be negligible compared to the similarity of their optical properties as has been suggested by previous experimental optical spectra.

Experimentally, optical properties of crystalline and noncrystalline SiO_2 in the energy range 0–26 eV were investigated by Philipp 40 years ago.[6,14,15] He observed similar optical properties for crystalline and fused quartz and found the spectral dependence of the real and imaginary parts of the dielectric constant on the composition value of x for SiO_x (x=0–2). Loh also measured the optical absorption in fused silica and that of quartz and found them to be very similar.[16] Bosio[17] and Sorok[18] reported the same optical properties of c-SiO_2 and a-SiO_2.[17] Tarrio reported similar optical properties for chemically vapor deposited (cvd) a-SiO_2 thin films, evaporated SiO_2 films, and bulk silica.[19] This has been con-

 ©2005 The American Physical Society

firmed by many later studies,[20,21] leading to the conviction that optical spectra in all SiO_2 phases with 4:2 coordination are the same. We have reported the complex optical properties of a-SiO_2 over the range of 1.5–42 eV, from which were observed additional interband transitions at 21.3 and 32 eV.[7] We found that a-SiO_2 has similar electronic structure to c-SiO_2 over a wide energy range.

Knowledge of the fundamental vacuum ultraviolet optical properties in crystalline and amorphous SiO_2 is important because high-purity synthetic SiO_2 crystals and glasses are important optical materials, being the basis for optical elements, optical fiber telecommunications, and photolithographic photomasks. We aim in this paper to present and compare optical spectra of crystalline and amorphous SiO_2 based on the vacuum ultraviolet spectra, the optical constants of c- and a-SiO_2, n and k, and the interband transition strength (J_{cv}). We augment the VUV reflectance measurements over the photon energy range of 2–40 eV using spectroscopic ellipsometry measurements to calibrate the optical constants over the low-energy wing between 0.69 and 8.0 eV. A procedure for simultaneously performing Kramers-Kronig dispersion analysis on the data from these two sources was described elsewhere.[22] The augmented data, spanning a wider energy range, leads to improved accuracy in amplitude, affording greater precision in determining and comparing the quantitative optical properties of crystalline and amorphous SiO_2.

The London dispersion interaction, the major component of the van der Waals forces,[23] is a universal, long-range interaction present for all materials, which arises directly from the electronic structure and optical properties of the materials.[24] Once the full spectral optical properties and electronic structure of bulk a-SiO_2 have been determined, the London dispersion interaction, and full spectral Hamaker constant[25] can be determined using the Lifshitz method.[26,27] When two grains of material 1 are separated by an intervening intergranular material, material 2, the Hamaker constant A_{121}^{NR} determines the magnitude of the London dispersion force (F_{LD}) between the two grains, as defined by Eq. (1). The intergranular material serves to shield the attraction of the two materials. The Hamaker constant is large for a vacuum interlayer, and zero if the interlayer material 2 is identical to the grain's material 1. The intimate relationship between the electronic structure and optical properties[28] and this universal interaction has attracted increased interest recently,[29] and the role of amorphous silica and other structural glass formers [such as SiON (Ref. 30) and $AlPO_4$ (Ref. 31)] as a fluid in high-temperature wetting and materials processes means a detailed knowledge of the optical properties and dispersion interaction in SiO_2 is of increased interest.

$$A_{121}^{NR} = -6\pi L^3 F_{LD} \tag{1}$$

II. EXPERIMENTAL METHODS

A. Sample preparation

Samples of crystalline and amorphous SiO_2 were used for the VUV and ellipsometry investigations. The amorphous SiO_2 samples studied here are of Suprasil 1.[32] This glass is homogeneous and free from striate in all directions, practically free from bubbles and inclusions, and characterized by a very high optical transmission in the UV and visible spectral ranges. The crystalline samples are either VALF X-cut (a quartz wafer with the major surface of the wafer perpendicular to the X crystallographic axis) or Z-cut (a quartz wafer with the major surface of the wafer perpendicular to the Z crystallographic axis) quartz.[33] Each sample was polished on both faces for spectroscopic ellipsometry and VUV optical measurement.

B. Spectroscopic ellipsometry

Spectroscopic ellipsometry was performed with the VUV-Vase instrument,[34] which has a range from 0.69 to 8.55 eV (1800–145 nm), and employs MgF_2 polarizers and analyzers rather than the more common calcite optics. The instrument has a MgF_2 autoretarder and is fully nitrogen purged. The spot diameter of light source on the surface of the sample is 2 mm. Ellipsometric measurements were conducted using light incident at angles of 60°, 70°, and 80° relative to normal on the front surface of the sample, the back of which was roughened with coarse polishing paper. The instrument measures the ellipsometric parameters Ψ and Δ, which are defined by Eq. (2),

$$\tan(\Psi)e^{i\Delta} = \frac{R_P}{R_S}, \tag{2}$$

where R_P/R_S is the complex ratio of the p- and s-polarized components of the reflected amplitudes. These parameters are analyzed using the Fresnel equations[35] in a computer-based modeling technique[34] including a surface roughness layer to directly determine the optical constants.

C. VUV spectroscopy

VUV spectroscopy has become an established technique for electronic structure studies of materials.[36–40] It has the advantage of covering the complete energy range of the valence interband transitions and is not plagued by the sample charging that attends photoelectron spectroscopy on insulators. The VUV spectrophotometer includes a laser plasma light source, a monochromator, filters and detectors.[41] The light source is not polarized, and the incident angle of the light on the sample is near normal. The details of the instrument have been discussed previously.[41,42] The energy range of the instrument is from 1.7 to 44 eV, or from 700 to 28 nm, which allows us to extend beyond the air cutoff of 6 eV and the window cutoff of 10 eV. The resolution of the instrument is 0.2–0.6 nm, which corresponds to 16 meV resolution at 10 eV or 200 meV resolution at 35 eV.

III. RESULTS

A. Analysis of ellipsometry data

The transmission spectra for both crystalline and amorphous SiO_2 within the VUV range are shown in Fig. 1. We use both ellipsometric and UV/vis transmission data taken on

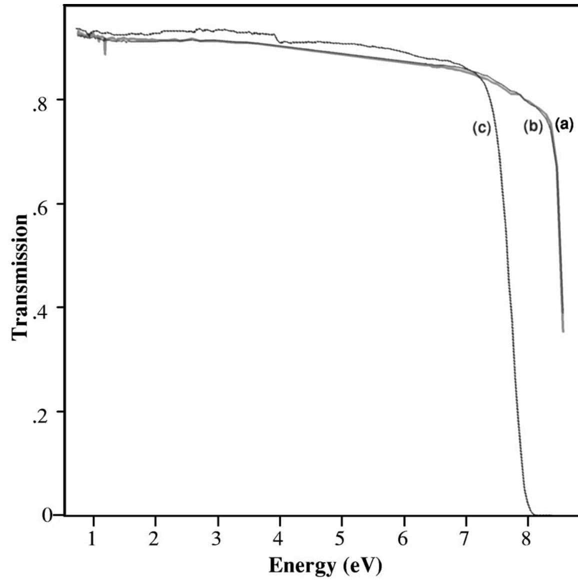

FIG. 1. Transmission of crystalline and amorphous SiO_2: (a) *X* cut, (b) *Z* cut, (c) a-SiO_2.

the same sample to find a model describing the optical behavior of the bulk silica.[35] Using transmission data and ellipsometric data in the modeling reduces the effective surface sensitivity of ellipsometry, while increasing the accuracy of the bulk properties. The complex index of refraction for both crystalline and amorphous SiO_2 within the energy range from 0.7 to 8 eV for this solution is shown in Fig. 2, which agree very well with literature results.[43]

B. Kramers-Kronig analysis of VUV reflectance

Accurate results from Kramers-Kronig analysis rely on the accurate determination of the amplitude of the VUV reflectance (shown in Fig. 3), and preparation of low- and high-energy wings which extend beyond the experimental data range. We prepare the low-energy wing, in the range

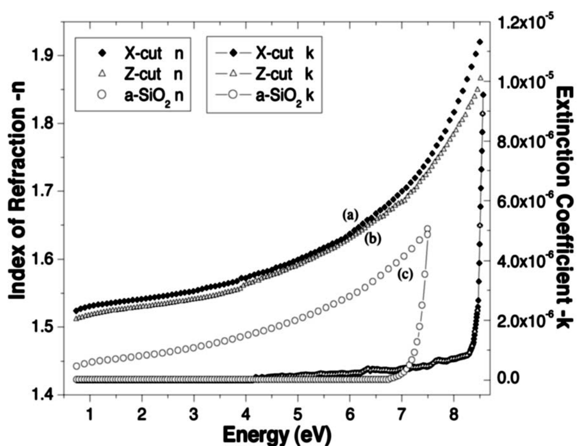

FIG. 2. Complex index of refraction, $\hat{n}=n+ik$, determined from spectroscopic ellipsometry for (a) *X*-cut quartz, (b) *Z*-cut quartz, (c) a-SiO_2. The index of refraction n is the dotted line, while the extinction coefficient k is the solid line.

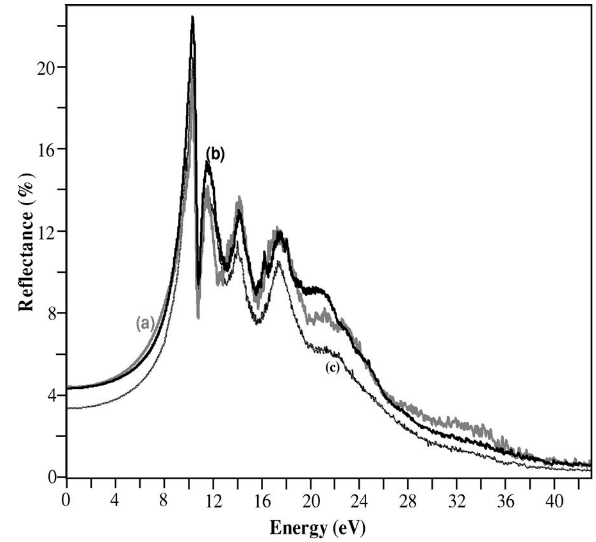

FIG. 3. Reflectance spectrum of VUV spectrum measured from (a) *X*-cut quartz, (b) *Z*-cut quartz, (c) a-SiO_2.

below the band gap of the material (in this case of SiO_2, for energies below 6 eV), using a two pole Sellmeier form, and fitting the reflectance, with this low-energy wing, to the ellipsometric data in a least-squares sense. In this manner we determine more accurately the reflectance amplitude and low-energy wing, which will be used as input in the Kramers-Kronig analysis. We also prepare and fit a high-energy wing for the reflectance. The details of these methods are discussed in detail in the Kramers-Kronig Analysis Appendix of our 1999 paper.[22] Kramers-Kronig analysis is then used to recover the reflected phase. In the case of normal incidence, the complex reflection coefficient is written in terms of the amplitude $\bar{R}$ and a phase shift upon reflection θ, as described by

$$\tilde{R} = |\bar{R}|e^{-i\theta} = \frac{n-1-ik}{n+1-ik}. \quad (3)$$

The complex index of refraction ($\hat{n}=n+ik$) for both crystalline and amorphous SiO_2 is then calculated algebraically from Eq. (3) and the results are shown in Fig. 4. It can be seen that the index of refraction and extinction coefficient values measured from spectroscopic ellipsometry (short course curves) agree with those calculated from VUV spectra through our Kramers-Kronig analysis procedures. They also agree with Palik's Handbook result of SiO_2 within this energy range.

The fundamental absorption-edge spectra have been determined by Eq. (4):[43]

$$\alpha = \frac{4\pi \mathrm{k}}{\lambda}, \quad (4)$$

where α is the absorption coefficient, λ is the wavelength of the light source, and k is the extinction coefficient. The fundamental absorption spectra for crystalline and amorphous SiO_2 are shown in Fig. 5 (from spectroscopic ellipsometry) and Fig. 6 (VUV spectrometer).

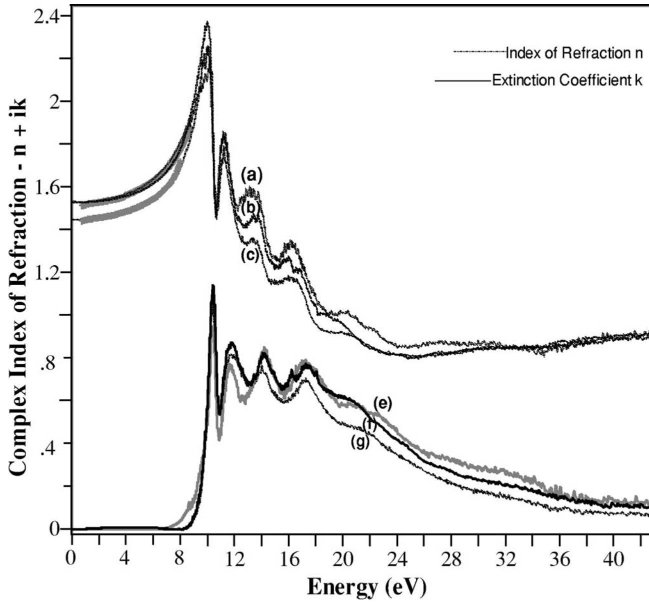

FIG. 4. Complex index of refraction, ($\mathbf{n}=n+ik$) of crystal and amorphous SiO_2, where the index of refraction n is shown by the dashed line and the extinction coefficient k by solid lines. (a) and (e) X-cut quartz, (b) and (f) Z-cut quartz, (c) and (g) a-SiO_2.

Here we render the optical response in terms of the interband transition strength $J_{cv}(E)$, related to $\varepsilon(\omega)$ by[24]

$$\hat{J}_{cv} \equiv J_{cv1} + iJ_{cv2} = \frac{m_0^2}{e^2\hbar^2}\frac{E^2}{8\pi^2}[\varepsilon_2(E) + i\varepsilon_1(E)], \qquad (5)$$

where $J_{cv}(E)$ is proportional to the transition probability and has units of g cm^{-3}. For computational convenience we take the prefactor in Eq. (5), whose value n cgs units is 8.289 $\times 10^{-6}$ g cm^{-3} eV^{-2}, as unity. Therefore the $J_{cv}(E)$ spectra calculated from Eq. (5) shown in Fig. 7 are in units of eV^2. The bulk energy-loss function (ELF) for both a-SiO_2 and c-SiO_2, ELF$=-$Im$[1/\varepsilon(\omega)]$, is shown in Fig. 8.

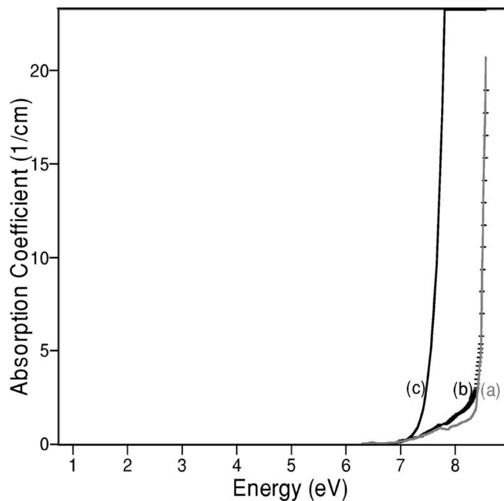

FIG. 5. Fundamental absorption edge of SiO_2 within low-energy range for (a) X cut, (b) Z cut, (c) a-SiO_2, which was determined from spectroscopic ellipsometry and subsequent Kramers-Kronig transformation of the index of refraction.

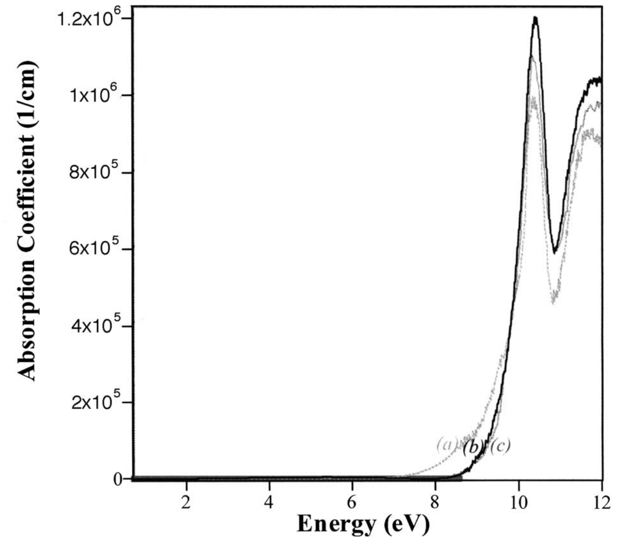

FIG. 6. Fundamental absorption edge of SiO_2: (a) a-SiO_2 (b) X-cut quartz, (c) X quartz within wider energy range. The absorption coefficient (α), in units of cm^{-1}, is plotted vs energy. The absorption spectra were extracted from VUV measurement.

The oscillator strength sum rule[44] [Eq. (6)] applied to the interband transition strength allows the determination of the number of electrons contributing to a transition up to an energy $E[n_{\text{eff}}(E)]$.

$$n_{\text{eff}}(E) = \frac{4\nu_f}{m_o}\int_0^E \frac{\text{Re}\{J_{cv}(E')\}}{E'}dE'. \qquad (6)$$

Here ν_f is the volume of the SiO_2 formula unit. The $n_{\text{eff}}(E)$ of the oscillator strength sum rule for crystalline and amorphous SiO_2 is shown in Fig. 9.

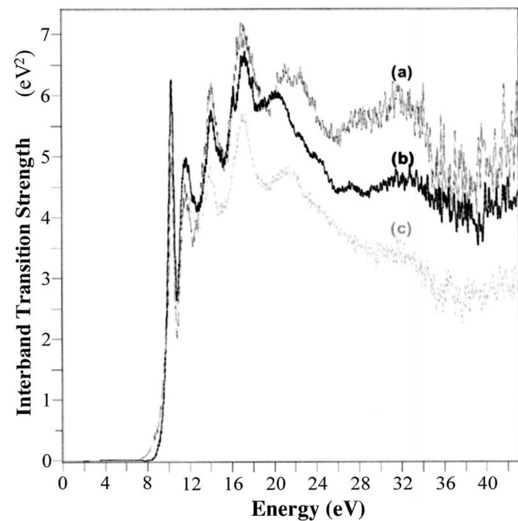

FIG. 7. Real part of the interband transition strength spectrum (Re$[J_{cv}]$) of quartz and amorphous SiO_2 determined from Kramers-Kronig analysis of VUV reflectance data. (a) X-cut quartz, (b) Z-cut quartz, (c) a-SiO_2.

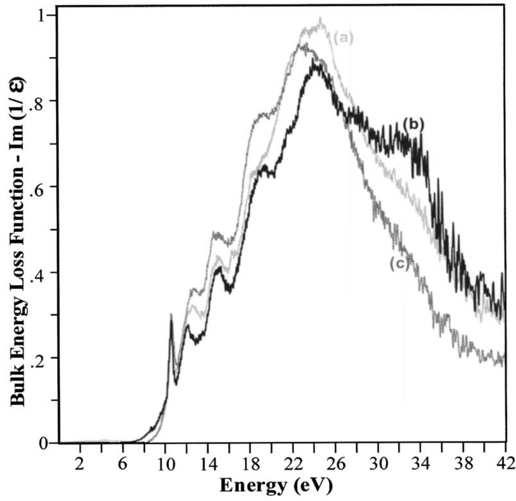

FIG. 8. Bulk electron-energy-loss function, $-\mathrm{Im}(1/\varepsilon)$, of (a) X-cut quartz, (b) Z-cut quartz, (c) a-SiO_2, showing the bulk plasmon resonance peaks.

C. Hamaker constants of the London dispersion interaction

To calculate the London dispersion interaction and its nonretarded Hamaker constant[24] we utilize another Kramers-Kronig dispersion relation to produce the London dispersion spectrum, $\varepsilon_2(i\xi)$, which is an integral transform of the imaginary part of the dielectric constant from the real frequency ω to the imaginary frequency $i\xi$. The London dispersion spectrum is a material's property and represents the retardation of the oscillators,

$$\varepsilon(i\xi) = 1 + \frac{2}{\pi}\int_0^\infty \frac{\omega\varepsilon_2(\omega)}{\omega^2+\xi^2}d\omega. \quad (7)$$

Therefore once the complex optical properties as a function of the real frequency ω have been determined, the London dispersion (LD) integral transform [Eq. (7)] yields the London dispersion spectrum. The LD transform requires data over an infinite frequency or energy range, and therefore we use analytical extension or wings to continue the data beyond the experimental data range. We choose power-law wings of the form $\mathrm{Re}[J_{cv}] \propto \omega^{-A}$ on the low-energy side of the data and $\mathrm{Re}[J_{cv}] \propto \omega^{-B}$ on the high-energy side of the data, where A and B are chosen values of $A=2$ and $B=3$. In determining the LD spectrum, we retain the complete spectrum over the entire 0–250 eV range to facilitate the evaluation of the spectral difference functions while minimizing errors resulting from neglected area between the $\varepsilon_2(\xi)$ spectra. The detailed methods for calculating the full spectral Hamaker constant can be found in French's review article.[24] Here we report the Hamaker constants for different configurations with amorphous and crystalline SiO_2 in Table I.

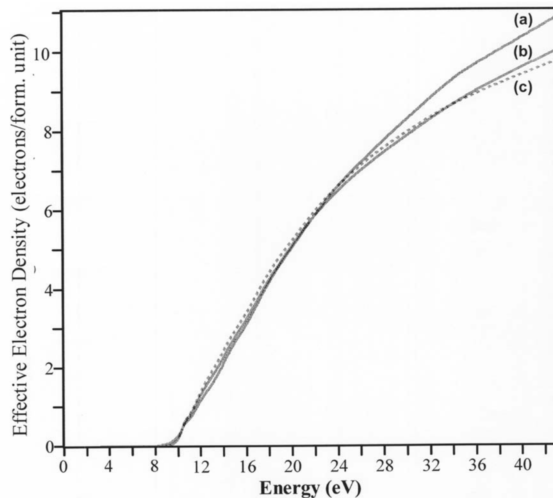

FIG. 9. Oscillator strength sum rule of crystal and amorphous SiO_2. (a) X-cut quartz, (b) Z-cut quartz, (c) a-SiO_2.

IV. DISCUSSION

A. Band gap

Reflectance spectra for crystalline and amorphous SiO_2, shown in Fig. 3, agree qualitatively with the optical transitions in other crystalline and amorphous silica reported by others.[14,15] It can be seen from Fig. 3 that the reflectivity peaks for both forms of SiO_2 are located at 10.4, 11.6, 14.03, and 17.10 eV, as reported previously. The experimentally determined absorption coefficient in the energy region of the fundamental absorption edge α (cm^{-1}), is shown in Fig. 5 from ellipsometric measurements and Fig. 6 from VUV measurements SiO_2. In Table II, the results of band-gap fitting are summarized for fits in two different ranges of the absorption coefficient. These experimentally determined direct band-gap energies are determined by a direct gap model using a linear fit in the absorption edge region of interest to a plot of α^2E^2, where α is the absorption coefficient in cm^{-1} and E is energy in eV. The band-gap energies for the indirect band-gap model are determined by linear fitting to $\alpha^{1/2}$. Direct and indirect band-gap models do not formally apply to amorphous materials such as glass, due to the loss of long-range periodicity in the amorphous material and the consequent destruction of the Brillouin-zone construct used for band-structure analysis. However, direct and indirect gap fitting has been used for characterizing the changes in the absorption edge in amorphous materials such as amorphous silicon[39] and other amorphous semiconductors[40] and has been found useful to characterize the observed changes in the electronic structure. Therefore we are using the direct and indirect models as useful tools to characterize the complex absorption-edge behavior of these materials, and draw on the crystalline band-gap models because the shapes of the absorption edges measured are reminiscent of those found in crystalline materials.[38]

The upper limit of the fitted direct band-gap values for X-cut quartz within the linear absorption region is about 9.34 eV corresponding to the absorption range within $\alpha \sim 1\times10^5$–1×10^6 cm^{-1}, while the indirect gap in this region is evaluated to be 8.30 eV. While that value for Z-cut quartz

TABLE I. Full spectral Hamaker constants A_{121}^{NR} or A_{123}^{NR} for the London dispersion interaction of different physical configurations with a-SiO$_2$ or c-SiO$_2$ as one component, determined from the interband transition strength spectra. (c-SiO$_2$: Z-cut quartz; a-SiO$_2$: amorphous SiO$_2$; EEL: calculation from EELS spectrum; VUV: calculation from VUV spectrum.)

Physical geometry	Ham. coeff.	Physical geometry	Ham. coeff.
[a-SiO$_2$|vacuum|a-SiO$_2$]	71.6zJ	[c-SiO$_2$|vacuum|c-SiO$_2$]	94.7zJ
[a-SiO$_2$|Al$_2$O$_3$|a-SiO$_2$]	24.6zJ	[c-SiO$_2$|Al$_2$O$_3$|c-SiO$_2$]	13.18zJ
[a-SiO$_2$|water|a-SiO$_2$]	8.0zJ	[c-SiO$_2$|water|c-SiO$_2$]	17.6zJ
[a-SiO$_2$|c-SiO$_2$|a-SiO$_2$]	17.3zJ	[c-SiO$_2$|a-SiO$_2$|c-SiO$_2$]	17.3zJ
[Si$_3$N$_4$|a-SiO$_2$|Si$_3$N$_4$]	38.2zJ	[Si$_3$N$_4$|c-SiO$_2$|Si$_3$N$_4$]	25.8zJ
[TiO$_2$|a-SiO$_2$|TiO$_2$]	33.2zJ	[TiO$_2$|c-SiO$_2$|TiO$_2$]	48.5zJ
[a-SiO$_2$|Al$_2$O$_3$|air]	64.1zJ	[c-SiO$_2$|Al$_2$O$_3$|air]	46.8zJ
[Al$_2$O$_3$|a-SiO$_2$|air]	−41.5zJ	[Al$_2$O$_3$|c-SiO$_2$|air]	−34.9zJ
[a-SiO$_2$|water|air]	−15.6zJ	[c-SiO$_2$|water|air]	−23.2zJ
[TiO$_2$|a-SiO$_2$|air]	−56.7zJ	[TiO$_2$|c-SiO$_2$|air]	−52.1zJ
⟨SrTiO$_3$|vacuum|SrTiO$_3$⟩^{EEL}	234.9zJ	⟨SrTiO$_3$|vacuum|SrTiO$_3$⟩^{VUV}	248.8zJ
⟨SrTiO$_3$|water|SrTiO$_3$⟩^{EEL}	110.5zJ	⟨SrTiO$_3$|water|SrTiO$_3$⟩^{VUV}	118.4zJ
⟨SrTiO$_3$|water|air⟩^{EEL}	−59.7zJ	⟨SrTiO$_3$|water|air⟩^{VUV}	−61.6zJ

within the linear absorption region is determined to be 9.55 eV (corresponding to the absorption range of $\alpha \sim 1\times10^5$–1×10^6 cm^{-1}), the indirect band-gap energy in the same absorption region is fitted to be 8.91 eV. Within the absorption edge region of 1×10^5–1×10^6 cm^{-1}, the direct band gap of amorphous SiO$_2$ was fitted to be 9.56 eV from the absorption edge, the indirect gap of which was evaluated to be 8.90 eV in the same absorption region. The band gaps of amorphous SiO$_2$ in the region of very low absorption coefficient (2–20 cm^{-1}) have been calculated from ellipsometric spectra to be 7.64 eV for direct transition and 7.46 eV for indirect transition, respectively. In the extremely low absorption region, the direct gap energies of c-SiO$_2$ have much higher values than a-SiO$_2$, determined from ellipsometric spectra within the region of 2–20 cm^{-1} in Fig. 5 to be 8.30 eV for X-cut quartz and 8.29 eV for Z-cut quartz. The indirect gaps are evaluated to be 8.12 eV for X-cut quartz and 8.05 eV for Z-cut quartz in the same absorption regions.

Weinberg *et al.*[45] as well as DiStefano and Eastman[5] have reviewed other experimental determinations of the direct band gap of SiO$_2$ and reported values of 9.3 and 9.0 eV for the band gap of a-SiO$_2$ from photoconductivity measurements. These values are comparable to the direct band-gap energies of either crystalline or amorphous SiO$_2$ in the high absorption coefficient results of Table II. The reason for the difference in the fitted band-gap energies between c-SiO$_2$ and a-SiO$_2$ in the extremely low absorption region is that Suprasil I a-SiO$_2$ has very high OH content (up to 1200 ppmw level), which produces a substantial quantity of 2≡Si-OH as discussed by Griscom.[46] This Si-OH group may play an important role in altering the direct band-gap energy for OH containing fused glass. With the presence of the Si-OH group, the band gap of fused SiO$_2$ decreases with increased OH content.[47] Meanwhile, absorption of the bulk specimen at around 7.9 eV has several possible origins including extrinsic impurities, intrinsic defects including oxygen deficient centers (ODCs), and strained Si-O-Si bonds in three- or four-member rings.[48]

B. Optical properties and interband transitions of crystalline and amorphous SiO$_2$

It can be seen from the reflectance spectra in Fig. 3 that both c-SiO$_2$ and a-SiO$_2$ share common reflectivity peaks at 10.4, 11.6, 14.03, and 17.10 eV, which agree with reported optical transitions for crystalline and amorphous silica.[14,15,18,49] According to Laughlin's[50] report, the peak at about 10.4 eV is due to an excitonic resonance in both

TABLE II. Results of band-gap fitting to the fundamental absorption edges of a-SiO$_2$ and c-SiO$_2$.

Sample	Direct gap	Abs. fitting range	Indirect gap	Abs. fitting range
Suprasil 1 amorphous SiO$_2$	7.64[a] eV	2–20 cm^{-1}	7.46[a] eV	2–20 cm^{-1}
	9.56 eV	1×10^5–1×10^6 cm^{-1}	8.90 eV	1×10^5–1×10^6 cm^{-1}
Crystalline SiO$_2$ X-cut quartz	8.30 eV[a]	2–20 cm^{-1}	8.12 eV[a]	2–20 cm^{-1}
	9.34 eV	1×10^5–1×10^6 cm^{-1}	8.30 eV	1×10^5–1×10^6 cm^{-1}
Crystalline SiO$_2$ Z-cut quartz	8.29 eV[a]	2–20 cm^{-1}	8.05 eV[a]	2–20 cm^{-1}
	9.55 eV	1×10^5–1×10^6 cm^{-1}	8.91 eV	1×10^5–1×10^6 cm^{-1}

[a]Calculated from spectroscopic ellipsometry.

c-SiO_2 and a-SiO_2, and has also been so identified by other authors.[15,18,49,51,52] As reported in earlier papers, the other three peaks at 11.6, 14.03, and 17.10 eV are due to interband transitions in both a-SiO_2 and c-SiO_2, which also agree in energy with the measurements of others.[14,15,19] By following Ibach's conclusion,[53] the 11.6 eV transition corresponds to an excitation from the valence-band maximum at −2.5 eV to the conduction-band edge, where we have set the zero of energy in the density of states to lie at the valence-band maximum. The remaining common features at 14.03, 17.3, 21.3, and 32 eV have been observed in the interbrand transition strength spectra ($\mathrm{Re}[J_{cv}]$ as defined in Eq. (5)) of both crystalline and amorphous SiO_2 (Fig. 7), which may be assumed to originate from the three principle maxima in both the valence-band density of states and the O 2s core state, terminating at an energy level near the conduction-band edge.[54] Specifically, these different interband transitions could be assigned from the band structure[54] of SiO_2 as follows: the feature at 14.03 eV is for the transition from the energy level at −3.9 eV in the valence band (VB) to the energy level at 10.13 eV in the conduction band (CB), the feature peak at 17.3 eV is for the transition from the VB, −6.5 eV, to the CB, 10.9 eV,[7] the feature peak at 21.3 eV is for the transition from the VB, −9.7 eV, to the CB, 11.6 eV, and the 32-eV feature peak is for the transition from the O 2s core level at −20.2 eV to a low-lying vacant state near the CB edge.[7]

Most of the prior experimental optical property results were obtained on either α-quartz or more frequently amorphous silica, in either the bulk glass or thin film forms. In α-quartz the Si-O bond length is 1.61 Å and the Si-O-Si angle is 144°.[55] In a-SiO_2 these two parameters have a random distribution, but their mean values are similar to those found in α-quartz. The SiO_4 tetrahedron, on the other hand, remains almost structurally perfect with only very small deviations in α-SiO_2 of the O-Si-O angle of 109.5°.[56] Thus the spectroscopic results for α-quartz and a-SiO_2 can be expected to exhibit similar features, some of which are characteristic of the SiO_4 tetrahedron and some which are more dependent on the mean Si-O-Si angle of 144°.[54] It can be concluded that it is the SiO_4 tetrahedron which is predominantly responsible for the electronic structure and optical transitions of both crystalline and amorphous phases of SiO_2.[14] From this, any differences between the electronic structure of crystalline and amorphous SiO_2 may be anticipated to arise from the main atomic structural feature: the random variation of the Si-O-Si angle in the amorphous form of SiO_2. Although the density of crystalline compared to amorphous SiO_2 is larger by about 1.2 times, the absorption per SiO_2 molecule or per Si-O bond is the same in both structural forms. It may therefore be supposed that the common structural units of an Si-(O_4) tetrahedron determine the optical properties of different forms of SiO_2, leading to the same characteristic optical spectra features: exciton resonance peak at 10.4 eV and interband transitions locating at 11.6, 14.3, 17.1, and 32 eV for both crystalline and amorphous SiO_2.

The difference of the optical properties for crystalline and amorphous SiO_2 comes from the variation of the Si-O-Si angle in SiO_4 tetrahedron as well as the orderly alignment of these tetrahedra, resulting in differences in the amplitude of the reflectivity and the refractive index among the different forms of SiO_2. Due to their higher physical density quartz samples have much higher reflectance and refractive indices than amorphous silica as shown in Figs. 3 and 4. There are also some differences amongst the quartz and amorphous samples themselves. Z-cut quartz has a higher value of the reflectance and refractive index than X-cut quartz. The short-range order (SRO) of amorphous SiO_2 is the same as in the 4:2 coordinated crystals. However, it is the intermediate range order (IRO) and the lack of long-range order (LRO) that distinguishes the a-SiO_2 from its crystalline counterpart. It had been reported that the calculated electronic density of states (DOS) of crystalline SiO_2 and amorphous SiO_2 have subtle differences, reflecting differences in the LRO and IRO of these two phases, in spite of the similarity in their SRO.[12] The long-range order is destroyed on transition from the periodic crystalline lattice to the more random amorphous state. Therefore the LRO and IRO make the interband transitions of crystalline SiO_2 exhibit sharper features than does the amorphous SiO_2 counterpart (as shown in Figs. 3 and 7), whose LRO had been destroyed and whose valence and conduction bands are consequently broadened. The difference between the interband transition strength of Z-cut and X-cut quartz may arise from the orientation of the crystal and the unpolarized nature of our vacuum ultraviolet laser plasma light source used for the reflectance measurement. Z-cut quartz has the c face on its surface and has [0001] orientation, and in-plane on the c face is the x-y plane, which is perpendicular to (0001) direction and is optically isotropic. While X-cut quartz keeps an a-face on its surface and has [1000] orientation, in-plane directions on an a face are the y-z plane, which is parallel to (0001) direction (z axis) and has anisotropic optical properties. This orientation difference between Z-cut and X-cut quartz gives rise to the difference in optical properties and interband transitions.

Different forms of SiO_2 exhibit obvious differences in the interband transition strength spectrum (Fig. 7), within the energy range of 20–23 eV. Amorphous SiO_2 forms share the common interband transition peak at 21.5 eV, while X-cut and Z-cut quartz have the same peak shifted to 22.6 eV. There are three special peaks for Z-cut quartz, located at 16.2, 20.1, and 27.5 eV, which have not been observed in other forms or orientation of SiO_2. X-cut quartz also has two special peaks at 21 and 22.6 eV, which is different from other forms or orientations.

As pointed out above, the DOS of different forms or orientations of SiO_2 differs only in the fine details, which reflect the differences in the LRO and IRO. There has been no detailed scrutiny in the literature for differences in the electronic structure and interband transitions between crystalline and amorphous SiO_2. We observe more features in the interband transition strength spectrum of c-SiO_2 than for a-SiO_2 (Figs. 3 and 7) which reveal several additional interesting features located at 16.2, 20.1, 21, 22.6, 27.5, and 32 eV in the reflectance spectra and interband transition strength spectra of crystalline Z-cut quartz, and these spectral features do not appear in a-SiO_2. The 27.5 eV peak can be assigned to an excitation transition from the O 2s lower valence-band state at −20.2 eV to an exciton state at 7.1 eV near the conduction band, when the zero of energy is chosen at the valence-band

maximum. It is worth mentioning that peaks lying within the 20–23 eV energy range in the interband transition strength spectra look like features observed in electron-energy-loss spectroscopy spectrum of SiO_2. Ibach[53] studied the electronic structure of oxygen adsorbed on silicon (111) surfaces and oxidized silicon by electron-energy-loss spectroscopy. He observed bulk plasma loss peak at 21.3 eV and two additional interband transition peaks at 23 and 32 eV for SiO_2. We observe in the VUV reflectance and interband transition strength spectra shown in Figs. 3 and 7 similar peaks at 20.1 and 22.6 eV for *Z*-cut quartz, 21 and 22.6 eV for *X*-cut quartz, and only 21.3 eV for amorphous SiO_2 as well as a 32 eV transition[7] in all forms of SiO_2. It seems clear that the 22.6 eV peak corresponds to an electronic transition from oxygen (DOS state at −17.6 eV to a final conduction-band state at 5.8 eV).[53] The remaining two peaks at 16.2 and 20.1 eV are only observed in *Z*-cut quartz spectra and also correspond to valence- to conduction-band transitions. We may assign the peak at 16.2 eV to the transition from the energy level at −2.5 eV in valence band to the level at 13.8 eV in conduction band, the other peak at 20.1 eV to be the transition from the energy level at −9.7 eV to the level at 10.6 eV below the edge of conduction band. It is reported that the 32 eV peak never appeared on a clean Si surface but was observed after oxygen absorption on a silicon (111) surface,[53] making this peak another oxygen associated transition. Therefore the peak at 32 eV in the interband transition strength is due to electronic transition from O 2*s* energy level to the lower conduction band in SiO_2.

The broad peak at 21.3 eV for *a*-SiO_2 and 22.6 eV for *c*-SiO_2 is near the energy positions of plasmon resonance peaks for SiO_2,[7] and can therefore be assigned as either an interband transition or the bulk plasma resonance peak. For the first case, the two peaks could correspond to an electronic transition from the oxygen valence-band to the conduction-band states, which may be confirmed by Ching's *ab initio* calculation of optical properties of SiO_2.[11] In order to discriminate the interband transition peaks from plasmon resonance peaks of either *a*-SiO_2 or *c*-SiO_2, it is useful to consider the bulk energy-loss functions of *a*-SiO_2 and *c*-SiO_2, $\mathrm{ELF}=-\mathrm{Im}[1/\varepsilon(\omega)]$ (shown in Fig. 8). The bulk plasmon resonance peaks in the ELF spectra are observed at 23.7 eV for amorphous SiO_2,[7] 24.6 eV for *X*-cut quartz, and 25.2 eV for *Z*-cut quartz. Similar ELF data were obtained by Maixner *et al.*,[49] whose results for amorphous SiO_2 for small wave vectors ($q=0.2$) are in good agreement with our ELF results of amorphous SiO_2. Thus the peaks in $\mathrm{Re}[J_{cv}]$ spectrum at 21.5 eV for *a*-SiO_2 and 22.6 eV for *c*-SiO_2 should be attributed to interband transitions, different from the plasmon collective excitation peaks which have been observed separately within the 23–25.2 eV energy range in the ELF spectrum of *a*-SiO_2 and *c*-SiO_2.

The expected value of oscillator strength sum rule for SiO_2 is 16 electrons per formula unit, consisting of eight O 2*p* electrons, four O 2*s* electrons, two Si 3*s* electrons, and two Si 3*p* electrons. The oscillator-strength sum rules n_{eff} for different forms of SiO_2 are shown in Fig. 9. These oscillator strength spectra indicate that 9.8 electrons per formula unit for amorphous SiO_2 as well as 10.8 electrons for *X*-cut quartz and 10.0 electrons for *Z*-cut quartz, respectively, have participated in their interband transitions at the energies at or below 43 eV. From Fig. 9(a) we can pick up a value of 7.3 electrons per formula unit for amorphous SiO_2 at 26 eV, which is very close to Philipp's[15] 7.7 electrons per *a*-SiO_2 molecule near 26 eV. There is no direct evidence this plot will saturate near 43 eV. Presumably transitions associated with the deeper-lying *L*-shell electrons of oxygen will be energetically possible at some higher energy and the curve will rise further. The physical density of *c*-SiO_2 (2.65 $\mathrm{g/cm^3}$) is higher than that of *a*-SiO_2 (2.201 $\mathrm{g/cm^3}$), therefore there are more valence electrons for *c*-SiO_2 in a unit volume than in *a*-SiO_2.

FIG. 10. Profile of two layers of *a*- (or *c*-) SiO_2 grains being separated by an interlayer film.

From the interband transition strength spectrum, reflectance, and the oscillator sum rule, we can see that the change from crystalline to amorphous SiO_2 tends to weaken the sharp spectral features seen in the interband transitions. *X*-cut quartz has the strongest interband transitions and the most valence electrons participating in the interband transitions, while amorphous SiO_2 has the weakest interband transition and the least electrons participating in the transition. This role of disorder on the electronic structure of SiO_2 has also been reported for *c*-SiO_2 in which the surface has been disordered by argon bombardment.[57]

C. London dispersion interaction for amorphous and crystalline SiO_2

The London dispersion interaction arises directly from the material's optical properties and electronic structure. Therefore we can now consider the LD interactions involving SiO_2 using the Lifshitz theory.[24,26,27] Here we report the full spectral, nonretarded Hamaker constants (A_{121}^{NR} and A_{123}^{NR}) in Table I for different physical configurations with *a*-SiO_2 or *c*-SiO_2. Consider a physical configuration for a full spectral, nonretarded Hamaker constant calculation that consists of two layers (grains 1 and 3) separated by an interlayer film (2). The grains and film can be composed of any materials. For the nonretarded Hamaker constant to be applicable, the film in this three-layer configuration should be very thin (<2 nm).

In a configuration where the 1 and 3 layers are the same material we have the symmetrical 121 case[24] (Fig. 10) which is applicable, for example, to intergranular films. For this configuration with the interlayer or intergranular film having different physical properties and electronic structure from the outer grains, it is of interest to determine the magnitude of the Hamaker constant. We can see big differences in the Hamaker constants for geometries containing *a*-SiO_2 and *c*-SiO_2. The accuracy of these full spectral, nonretarded Hamaker constants is 3%, as we have determined from studies of variations in magnitude of the input spectra,[58] and by comparison to Hamaker constants determined from multiple

approaches[59] such as different approximate models (e.g., Tabor Winterton), or fitting to AFM force-distance curves.[60] In addition we show Hamaker constants calculated for $SrTiO_3$ using spectra determined from two experimental methods, electron-energy-loss spectroscopy and VUV spectroscopy,[61,62] and the results are in this 3% accuracy range. The Hamaker constant for the configuration of two a-SiO_2 films separated by vacuum (A^{NR}_{1v1}) is 71.6 zJ (Table I), while that of c-SiO_2 (Z-cut quartz) films separated by vacuum is 94.7 zJ. For a case of importance to aqueous colloid chemistry,[59] note that when separating two layers of a-SiO_2 with water, the Hamaker constant is 8.0 zJ, but when c-SiO_2 is separated by water, the Hamaker constant is 17.6 zJ. When an interlayer material of Al_2O_3 (Ref. 63) separates two layers of a-SiO_2, then the Hamaker constant (A^{NR}_{121}) is reduced from 71.6 zJ to 24.6 zJ, corresponding to a reduction in the London dispersion interaction by a factor of 2.5. Due to this interlayer film, when two layers of crystal SiO_2 are separated by an interlayer film of Al_2O_3, the Hamaker constant is 13.2 zJ. If the materials of the grains and the boundary are exchanged, the Hamaker coefficient remains the same. When a-SiO_2 separates two layers of Si_3N_4 (Ref. 30) containing 80 ppm CaO, the Hamaker constant is calculated to be 38.2 zJ, but with c-SiO_2 replacing a-SiO_2 in this configuration, the Hamaker coefficient changes to 25.8 zJ. When two layers of TiO_2 (Ref. 58) are separated by a-SiO_2, the Hamaker constant is 33.2 zJ, which increases to 48.5 zJ when c-SiO_2 replaces a-SiO_2.

In contrast to the symmetrical 121 configuration, asymmetrical 123 configurations can represent surficial films (layer 2) with layer 3 taken as air. In the case of a wetting condition, the dispersion force is repulsive, represented by the Hamaker constant being of negative sign, and layer 2 will thicken. For example, the Hamaker constant of a surficial layer of a-SiO_2 film on an Al_2O_3 substrate is −41.5 zJ while that of c-SiO_2 film on Al_2O_3 is −34.9 zJ. In both cases, SiO_2 films have a London dispersion interaction corresponding to wetting on the Al_2O_3 substrate, but a-SiO_2, with a larger negative Hamaker constant, has a larger dispersion free energy for wetting on Al_2O_3 surface than does c-SiO_2. We may conclude that a-SiO_2 has a higher London dispersion interaction for wetting than does c-SiO_2 for SiO_2 film on Al_2O_3 substrates. In the reverse case of a surficial film of Al_2O_3 on a SiO_2 substrate, one finds a nonwetting dispersion interaction for either crystalline or amorphous SiO_2 substrates because the Hamaker coefficients are positive, being 64.1 zJ for a-SiO_2 substrate and 46.8 zJ for a c-SiO_2 substrate. A surficial film of a-SiO_2 on a TiO_2 substrate has a larger London dispersion interaction for wetting than does c-SiO_2, because the Hamaker constant of a-SiO_2 on this substrate is −56.7 zJ, while that of c-SiO_2 is −52.1 zJ. For a surficial film of water on an a-SiO_2 substrate the Hamaker coefficient is −15.60 zJ, while on a c-SiO_2 substrate the Hamaker coefficient is −23.2 zJ, implying that the London dispersion interaction for wetting by water is larger for surficial films on quartz than on amorphous SiO_2 glass.

V. CONCLUSIONS

Kramers-Kronig dispersion analysis of reflectance data, combined with spectroscopic ellipsometry, yields improved accuracy in determining the quantitative VUV optical properties from 0.7 to 43 eV for both crystalline SiO_2 (Z-cut quartz and X-cut quartz) and amorphous SiO_2. Besides the VUV reflectance spectrum and dielectric constants, we have also derived the complex index of refraction, interband transition strength ($\mathrm{Re}[J_{cv}]$), oscillator strength sum rule, energy-loss function, and London dispersion spectra for the different forms of SiO_2. Crystalline SiO_2 shares common interband transition peaks with amorphous SiO_2 as previously reported at 10.4, 11.6, 14.03, and 17.10 eV. The similarity of the optical properties between crystalline and amorphous SiO_2 arises from their common structural unit, the $-SiO_4$ tetrahedron. From VUV optical spectra, we found four different interband transition peaks for Z-cut quartz at 16.2, 20.1, 22.6, and 27.5 eV which are not observed in other forms of SiO_2. X-cut quartz has two different peaks at 21 and 22.6 eV, while amorphous SiO_2 has one at 21.5 eV. In addition, c-SiO_2 has a higher value of reflectivity intensity, index of refraction and dielectric constants than a-SiO_2. The bulk plasma peaks in energy-loss function spectra derived from VUV optical spectrum are observed at 25.2 eV for Z-cut quartz, 24.6 eV for X-cut quartz, 23.7 eV for amorphous SiO_2, respectively. These differences in the electronic structure and optical properties, and the physical density of crystalline and amorphous SiO_2 can be attributed to differences in the intermediate-range order and long-range order of the different forms of SiO_2. The intimate relationship between the electronic structure and optical properties and the London dispersion interaction has attracted increased interest recently, and the role of amorphous silica and other structural glass formers as a fluid in high-temperature wetting and materials processes means a detailed knowledge of the optical properties and London dispersion interaction in SiO_2 is relevant. Hamaker constants for the London dispersion interaction of the configuration of two layers of c-SiO_2 or a-SiO_2 separated by an interlayer film have been determined, using full spectral methods, from the interband transition strength. The London dispersion interaction is appreciably larger in c-SiO_2 than a-SiO_2 due to the increased physical density, index of refraction, transition strengths, and oscillator strengths in quartz.

ACKNOWLEDGMENTS

We are grateful to Dr. L. K. Denoyer for software development, M. K. Yang for help with the spectroscopy, and B. B. French for editing the manuscript. This work was partially funded by NSF Award No. DMR-0010062 in cooperation with EU Commission Contract No. G5RD-CT-2001-00586.

*Corresponding author. Email address: roger.h.french@usa.dupont.com; URL: http://www.lrsm.upenn.edu/~frenchrh/index.htm

[1] G. Wiech, Solid State Commun. **52**, 807 (1984).
[2] J. E. Rowe, Appl. Phys. Lett. **25**, 576 (1974).
[3] R. Williams, Phys. Rev. **140**, A569 (1965).
[4] A. Koma and R. Ludeke, Phys. Rev. Lett. **35**, 107 (1975).
[5] T. H. Distefano and D. E. Eastman, Solid State Commun. **99**, 2259 (1971).
[6] H. R. Philipp, Solid State Commun. **4**, 73 (1966).
[7] G. L. Tan, M. F. Lemon, and R. H. French, J. Am. Ceram. Soc. **86**, 1885 (2003).
[8] T. A. Stephenson and N. J. Binkowski, J. Non-Cryst. Solids **22**, 399 (1976).
[9] M. L. Bortz and R. H. French, Appl. Spectrosc. **43**, 1498 (1989).
[10] David R. Lide, *Handbook of Chemistry and Physics* (CRC Press, LLC, Boca Raton, Florida, 2004), pp. 4–82.
[11] Y. N. Xu and W. Y. Ching, Phys. Rev. B **44**, 11048 (1991).
[12] M. Z. Huang, L. Ouyang, and W. Y. Ching, Phys. Rev. B **59**, 3540 (1991).
[13] Y. P. Li and W. Y. Ching, Phys. Rev. B **31**, 2172 (1985).
[14] H. R. Philipp, J. Non-Cryst. Solids **8-10**, 627 (1972).
[15] H. R. Philipp, J. Phys. Chem. Solids **32**, 1935 (1971).
[16] E. Loh, Solid State Commun. **2**, 269 (1964).
[17] C. Bosio, G. Harbeke, W. Czaja, and E. Meier, Helv. Phys. Acta: **62**, 748 (1989).
[18] O. M. Sorokin and V. A. Blank, Opt. Spectrosc. **41**, 353 (1973).
[19] C. Tarrio and S. E. Schnatterly, J. Opt. Soc. Am. B **10**, 952 (1993).
[20] Yu. M. Alexandrov, V. M. Vishbjakov, V. N. Makhov, K. K. Siderin, A. N. Trukhin, and M. N. Ykimenko, Nucl. Instrum. Methods Phys. Res. A **282**, 580 (1989).
[21] J. E. Rowe, Appl. Phys. Lett. **25**, 576 (1974).
[22] D. J. Jones, R. H. French, H. Muellejans, S. Loughin, A. D. Dorneich, and P. F. Carcia, J. Mater. Res. **14**, 4337 (1999).
[23] J. D. van der Waals, originally published in Dutch in Verh. K. Akad. Wet. Amsterdam, **1**, 8 (1893), translation published by J. S. Rowlinson, J. Stat. Phys. **20**, 200 (1979).
[24] R. H. French, J. Am. Ceram. Soc. **83**, 2117 (2000).
[25] H. C. Hamaker, Physica (Amsterdam) **4**, 1058 (1937).
[26] E. M. Lifshitz, Sov. Phys. JETP **2**, 73 (1956) [Zh. Eksp. Teor. Fiz. **29**, 94 (1955).
[27] I. E. Dzyaloshinskii, E. M. Lifshitz, and L. P. Pitaevskii, Adv. Phys. **10**, 165 (1961).
[28] R. H. French, J. Am. Ceram. Soc. **73**, 477 (1990).
[29] K. van Benthem, G. Tan, L. K. DeNoyer, R. H. French, and M. Rühle, Phys. Rev. Lett. **93**, 227201 (2004).
[30] R. H. French, H. Müllejans, D. J. Jones, G. Duscher, R. M. Cannon, and M. Rühle, Acta Mater. **46** 7, 2271 (1998).
[31] G. L. Tan and R. H. French (unpublished).
[32] *Heraeus Suprasil Synthetic Glass*, Bes Optics, Inc., 1454 Main Street, W. Warwick, RI 02893, USA.
[33] Valpey Fisher Corporation, 75 South Street, Hopkinton, MA 01748, USA.
[34] *Woollam Spectroscopic ellipsometer*, J. A. Woollam Co., Inc., 645 M Street, 102 Lincoln, NE 68508, USA.
[35] B. Johs, R. H. French, F. D. Kalk, W. A. McGahan, and J. A. Woollam, Proc. SPIE **2253**, 1098 (1994).
[36] Y. N. Xu, W. Y. Ching, and R. H. French, Phys. Rev. B **48**, 17695 (1993).
[37] R. H. French, S. J. Glass, F. S. Ohuchi, Y.-N. Xu, and W. Y. Ching, Phys. Rev. B **49**, 5133 (1994).
[38] R. H. French, D. J. Jones, and S. Loughin, J. Am. Ceram. Soc. **77**, 412 (1994).
[39] R. H. French and J. B. Blum, Ceram. Trans. **7** (38), 111 (1990).
[40] K. van Benthem, C. Elsässer, and R. H. French, J. Appl. Phys. **90** (3), 6156 (2001).
[41] M. L. Bortz and R. H. French, Appl. Phys. Lett. **55**, 1955 (1989).
[42] R. H. French, Phys. Scr. **41**, 404 (1990).
[43] H. R. Philipp, *Handbook of Optical Constants of Solids*, edited by E. D. Palik (Academic, New York, 1985), Vol. I, p. 753.
[44] D. Y. Smith, *Handbook of Optical Constants of Solids* (Ref. 43), Vol. I, p. 35.
[45] Z. A. Weinberg, G. W. Rubloff, and E. Bassous, Phys. Rev. B **19**, 3107 (1979).
[46] D. L. Griscom, J. Ceram. Soc. Jpn. **99**, 923 (1991).
[47] R. H. French, R. A. Rahme, D. J. Jones, and L. E. McNeil, Ceram. Trans. **28**, 63 (1992).
[48] H. Hosono and Y. Ikuta, Nucl. Instrum. Methods Phys. Res. B **166**, 691 (2000).
[49] A. E. Meixner, P. M. Platzman, and M. Schlueter, *The Physics of* SiO_2 *and its Interfaces*, edited by S. T. Pantelides (Pergamon, New York, 1978), p. 85.
[50] R. B. Laughlin, Phys. Rev. B **22**, 3021 (1980).
[51] A. J. Bennett and L. M. Roth, Phys. Rev. B **4**, 2686 (1971).
[52] Y. M. Alexandrov, V. M. Vishnjakov, V. N. Makhov, K. K. Sidorin, A. N. Trukhin, and M. N. Yakimenko, Nucl. Instrum. Methods Phys. Res. A **282**, 580 (1989).
[53] H. Ibach and J. E. Rowe, Phys. Rev. B **10**, 710 (1974).
[54] D. L. Griscom, J. Non-Cryst. Solids **24**, 155 (1977).
[55] R. W. G. Wyckoff, *Crystal Structures* (Interscience, New York, 1965), Vol. 1, p. 321.
[56] D. L. Griscom, Phys. Rev. B **22**, 4192 (1980).
[57] J. E. Rowe and H. Ibach, Phys. Rev. Lett. **31**, 102 (1973).
[58] R. H. French, R. M. Cannon, L. K. DeNoyer, and Y.-M. Chiang, Solid State Ionics **75**, 13 (1995).
[59] H. D. Ackler, R. H. French, and Y. M. Chiang, J. Colloid Interface Sci. **179**, 460 (1996).
[60] C. Argento and R. H. French, J. Appl. Phys. **80**, 6081 (1996).
[61] K. van Benthem, R. H. French, W. Sigle, C. Elsässer, and M. Rühle, Ultramicroscopy **86** (3,4), 303 (2001).
[62] K. van Benthem, C. Elsässer, and R. H. French, J. Appl. Phys. **90** (12), 6156 (2001).
[63] R. H. French, H. Müllejans, and D. J. Jones, J. Am. Ceram. Soc. **81** (10), 2549 (1998).